Volume 336, number 3, 457–461 FEBS 13446 December 1993

Relaxation study of the backbone dynamics of human profilin by two-dimensional ^{1}H-^{15}N NMR

Keith L. Constantine[a,*], Mark S. Friedrichs[a], Aneka J. Bell[b], Thomas B. Lavoie[b], Luciano Mueller[a], William J. Metzler[a,*]

[a]*Department of Macromolecular NMR,* [b]*Department of Macromolecular Biochemistry, Bristol-Myers Squibb Pharmaceutical Research Institute, P.O. Box 4000, Princeton, NJ 08543-4000, USA*

Received 29 October 1993; revised version received 10 November 1993

The dynamic properties of 111 backbone HN sites in uncomplexed human profilin, a protein of 139 residues, have been characterized by two-dimensional inverse-detected ^{1}H-^{15}N NMR spectroscopy. Heteronuclear $\{^{1}H\}$-^{15}N nuclear Overhauser effects and ^{15}N longitudinal and transverse relaxation rates have been analyzed in terms of model-free spectral density functions and exchange contributions to transverse relaxation rates. Relatively high mobilities on the nanosecond timescale are observed for Asp^{26} and Ser^{27}, which form part of a loop connecting β-strands A and B, and for Thr^{92} through Ala^{95}, which are in a loop connecting β-strands E and F. Significant exchange contributions, indicative of motions on the microsecond to millisecond timescale, have been obtained for 30 residues. These include Leu^{77}, Asp^{80} and Gly^{81} of a loop between β-strands D and E, Ser^{84} and Met^{85} of β-strand E, Gly^{121} of a loop connecting β-strand G and the C-terminal helix, and Gln^{138}, which is next to the C-terminal residue Tyr^{139}. Some of the regions showing high flexibility in profilin are known to be involved in poly-L-proline binding.

Actin-binding protein; Conformational change; NMR relaxation; Order parameter; Poly-L-proline binding

1. INTRODUCTION

Profilin is a small cytoplasmic protein involved in the regulation of the phosphatidylinositol cycle, actin polymerization and, consequently, cytoskeletal rearrangement [1–4]. A ubiquitous protein, profilin occurs in a great variety of eukaryotic cells. Profilin interacts with a number of cellular components, including monomeric actin. In vitro, profilin has been demonstrated to bind phosphatidylinositol 4,5-bisphosphate (PIP_2) [5,6]. These observations implicate profilin as a central component in the signal transduction pathway leading to reorganization of the cytoskeleton. Profilin also binds poly-L-proline (PLP) [7–9]. While the biological significance of this latter interaction is unknown, the high occurrence of oligoproline stretches in cellular proteins** [9] indicates that PLP-binding is related to some as yet undiscovered function(s).

We have undertaken NMR studies of human profilin, a ~ 15 kDa protein containing 139 residues. Sequential ^{1}H, ^{13}C and ^{15}N NMR assignments, the elements of secondary structure, and a medium resolution tertiary structure have been determined [10]. Structural studies of profilins from other species are underway in several laboratories. X-ray crystallography is being applied to *Acanthamoeba* profilin-I [11] and the bovine profilin/actin complex [12,13]. Torchia and co-workers have reported NMR assignments, secondary structure elements, and a medium resolution tertiary structure for *Acanthamoeba* profilin-I [14,15]. Overall, the tertiary structures of human profilin [10] and *Acanthamoeba* profilin-I [15] are quite similar. Human profilin contains a seven-stranded antiparallel β-sheet, with the strands designated A through G. In addition, α-helices are located in the N- and C-terminal regions, and between β-strands B and C. The N- and C-terminal helices lie in an antiparallel fashion on one side of the β-sheet. NMR studies revealed that PLP binds in a hydrophobic cleft formed by the interface of the terminal ends of the N- and C-terminal helices and β-strands A, B, F and G [9]. Consistent with these results are mutagenesis data [9,16] which implicate a cluster of hydrophobic residues in PLP-binding.

In this paper, we report a study of the backbone dynamics of uncomplexed human profilin using two-dimensional (2D) inverse detected ^{1}H-^{15}N NMR methods [17–19]. ^{15}N T_1 and T_2 relaxation times and steady state $\{^{1}H\}$-^{15}N NOE values have been measured for 111 residues with adequately resolved ^{1}H-^{15}N correlations. These data are interpreted in terms of model-free spectral density functions [20–22] and exchange contributions to transverse relaxation rates. Several regions are found to have relatively high flexibilities on the ps–ns

*Corresponding authors. Fax: (1) (609) 252 6012.

**Over 200 protein sequences with contiguous stretches of six or more prolines have been identified [9]. These include phosphatases (e.g. calcinuerin A type II), kinases (e.g. KYK1 protein-tyrosine kinase-1), receptors (e.g. androgen receptor) and transcription regulators (e.g. FOS-B).

or μs–ms timescales; these include exposed loops that are sensitive to PLP binding [9].

2. EXPERIMENTAL

A uniformly ^{15}N-labeled NMR sample of human profilin was prepared as described elsewhere [9,10]. The sample used for the relaxation measurements was concentrated to 2.0 mM in a final volume of 0.6 ml, purged and sealed under argon. The buffer (pH 6.4) contained 10% ^2H_2O, 10 mM phosphate, 25 mM KCl, 20 mM β-mercaptoethanol, and 1 mM EDTA.

^{1}H-^{15}N NMR experiments were recorded at 20°C using a Varian UNITY-600 spectrometer. The spectra were acquired with the carrier frequencies set to 4.85 ppm (^{1}H) and 119.5 ppm (^{15}N), and with spectral widths of 8,000 Hz (^{1}H) and 1,600 Hz (^{15}N). The pulse sequence used for measurement of the steady-state {^{1}H}-^{15}N NOEs is given in [18], and those used for determining ^{15}N T_1 and T_2 relaxation times are described in [19]. All spectra were recorded as 128 t_1 increments with 1,024 complex points in t_2. For the ^{15}N T_1 and T_2 experiments, 32 transients were recorded per t_1 increment, and a recycle delay of 3.0 s was used. The NOE data (with and without ^{1}H saturation) were collected with 64 transients per t_1 increment using a recycle delay of 4.0 s. Longitudinal relaxation delays of 48, 160, 321, 481, 641, 882 and 1,123 ms were used for the T_1 experiments, and transverse relaxation delays of 7.8, 23.4, 39.0, 54.6, 70.2, 93.6 and 124.7 ms were used for the T_2 experiments. The 48 ms T_1 experiment was repeated twice (at the beginning and end of the data acquisition run) to assist in the determination of errors in the measured peak heights, and to verify sample stability. For all spectra, the time-domain data were processed to yield 1,024 real (F_1) by 1,024 real (F_2) point frequency-domain data matrices, with the upfield half of the ^{1}H acquisition dimension discarded. Additional details on NMR data acquisition and processing are as described in a previously reported ^{15}N relaxation study of an isolated antibody V_L domain [23].

The crosspeak heights derived from the T_1 and T_2 experiments were fit to exponential decays using methods described previously [23]. Errors in the peak heights for each residue were set equal to the root-mean-square baseline noise plus a percentage of the peak height at the shortest relaxation delay. Errors in derived T_1 and T_2 values were determined from 300 simulated peak height data sets derived from Gaussian random distributions about the experimental peak heights. The NOE values were derived from the ratios of crosspeak heights from experiments recorded with and without ^{1}H saturation ($NOE = I_{sat}/I_{unsat}$). Due to potential systematic errors [23], the NOEs are considered accurate to only ± 0.10 NOE units.

Dipolar and chemical shift anisotropy contributions to the ^{15}N longitudinal relaxation rates ($R_1 = 1/T_1$), transverse relaxation rates ($R_2 = 1/T_2$) and the {^{1}H}-^{15}N NOEs were considered, using the usual expressions [18,22–24] and previously defined values for physical constants [23]. An additional term (R_{2ex}) was in some instances added to the expression for R_2. Three different model-free spectral density functions, $J(\omega)$ [20–22], were used to numerically fit [23,25] the relaxation data:

$$J(\omega) = S^2\tau_r/(1 + \omega^2\tau_1^2) \quad (1)$$

$$J(\omega) = S^2\tau_r/(1 + \omega^2\tau_r^2) + (1 - S^2)\tau/(1 + \omega^2\tau^2) \quad (2)$$

$$J(\omega) = S_f^2S_s^2\tau_r/(1 + \omega^2\tau_1^2) + S_f^2(1 - S_s^2)\tau_s'/(1 + \omega^2\tau'^2_s) \quad (3)$$

where S^2 is the total generalized order parameter (which depends on the amplitudes of ps–ns motions), τ_r is the overall molecular rotational correlation time, τ is an effective correlation time resulting from internal motions characterized by a single internal correlation τ_i ($1/\tau = 1/\tau_i + 1/\tau_r$), S_f^2 and S_s^2 are order parameters corresponding to fast and slow internal ps–ns motions with timescales differing by at least an order of magnitude, respectively (note: $S^2 = S_f^2S_s^2$), and τ_s' is an internal correlation time resulting from the slower internal motions characterized by a slow correlation time τ_s ($1/\tau_s' = 1/\tau_s + 1/\tau_r$). In the following, τ_i and τ_s are both referred to as the effective internal correlation time τ_e. The criteria used for deciding which spectral density function to use for each fit, and whether or not to include R_{2ex}, have been described elsewhere [23]. Errors in the fitted parameters were determined by generating 200 Gaussian random distributions of the primary relaxation data for each residue and repeating the fits.

3. RESULTS AND DISCUSSION

Excluding the N-terminus, there are 134 backbone HN sites in human profilin. Of these, 93 are well resolved, displaying crosspeaks with either no overlap or only minor overlap with other crosspeaks in the 2D ^{1}H-^{15}N correlation spectra. Another 18 residues yield moderately overlapped crosspeaks for which peak height measurements were still feasible. Severe crosspeak overlap is observed for 23 residues, precluding characterization of these sites.

Fits of the T_1 values, using all 7 time points, were obtained for all 111 characterized residues. The T_1 data generally fit exponential decays very well. Excluding Gly^{121}, which yields very weak ^{1}H-^{15}N crosspeaks due to an exchange-broadening process (see below), all residues have maximum errors between the experimental and best-fit peak intensities that are < 4% of the corresponding derived equilibrium magnetization. The majority of residues have maximum T_1 data intensity errors that are < 1%. The average T_1 value is 840 ± 37 ms, and the maximum and minimum values are 1,020 ± 43 ms (Gly^{93}) and 755 ± 28 ms (Ser^{56}), respectively.

Fits of the T_2 values, using all 7 time points, were obtained for 107 of the 111 residues. Four residues – Asp^{80}, Gly^{81}, Ser^{84} and Gly^{121} – show both rapid T_2 relaxation and weak crosspeaks; therefore, the T_2 fits for these residues had to be performed using only the first few time points, resulting in somewhat less accurate parameter determinations. All 107 residues fit with 7 time points have maximum errors < 6%, and the majority have maximum errors < 2%. The average, maximum and minimum T_2 values are, respectively, 70 ± 13 ms, 137 ± 10 ms (Thr^{92}) and 29 ± 10 ms (Asp^{80}). Including only the 93 residues with well resolved crosspeaks yields an average T2 value of 72 ± 13 ms. The average NOE value for the 93 well resolved residues is 0.82 ± 0.10, with a number of residues exceeding the theoretical maximum of 0.83. As discussed elsewhere [23], this is likely due to partial ^{1}HN saturation caused by magnetization transfer from presaturated ^1H_2O and nearby saturated Hα resonances during the experiment recorded without broadband ^{1}H saturation. The minimum observed backbone {^{1}H}-^{15}N NOE is 0.24 for Ser^{27}. Plots of the primary relaxation data (T_1, T_2 and NOE values) vs. the sequential residue numbers are shown in Fig. 1. A table containing the primary relaxation data and their associated errors is available as supplementary material.

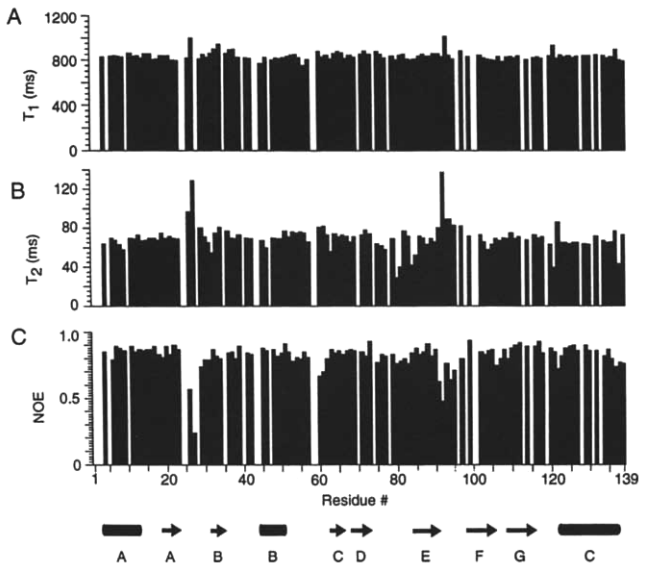

Fig. 1. Histograms summarizing the primary relaxation data obtained for human profilin at 20°C. Panel A: ^{15}N T_1 values. Panel B: ^{15}N T_2 values. Panel C: $\{^1H\}$-^{15}N NOE values. All panels show a value of 0 for residues that were not characterized. Residue numbers are displayed along the horizontal axis of the lower panel. The locations of the elements of secondary structure are indicated along the bottom of the figure, with barrels denoting the α-helices and arrows denoting the β-sheets.

An overall τ_r of 10.6 ± 0.2 ns has been determined from the T_1/T_2 ratios of 61 residues with well resolved crosspeaks which display an NOE ≥ 0.80 and T_2 > 66 ms. These criteria indicate residues for which both significant ps–ns timescale motions and significant μs–ms timescale motions are unlikely. The same average τ_r is obtained using residues with a T_1/T_2 ratio within one standard deviation of the mean T_1/T_2 ratio for the 93 well resolved residues. The overall rotational motion of profilin is expected to be highly isotropic, since the principal components of the inertial tensor, derived using the coordinates of the best NMR structure from the current ensemble [10], are 1.18:1.05:1.00. The overall τ_r of profilin (10.6 ns at 20°C) is larger than those observed for the ~ 17 kDa protein staphylococcal nuclease (9.1 ns at 35°C) [18] and for the ~ 18 kDa protein interleukin-1β (8.3 ns at 36°C) [22]. This difference is probably due to the significantly lower temperature used in the present study; however, minor aggregation of profilin can not be ruled out completely.

The derived τ_r was treated as a fixed parameter for the subsequent data analysis. Using the previously described criteria for selecting the model-free parameters to include in fitting the primary relaxation data to spectral densities [23], adequate fits were obtained for 106 residues. For these cases, the resulting model-free parameters reproduced T_1 and T_2 values within 3% of the experimental values, and NOEs within 0.10 of the experimental values. For residues 80, 81 and 121, less reliable fits were obtained due to the above mentioned exchange-broadening effects. Val^{51} and Ser^{56}, which were originally fit with Eqn. **(1)**, required Eqn. **(3)** for adequate fits. A table listing the functional form of the spectral density used for each residue, the derived model-free parameters, and their associated errors, is available as supplementary material. In cases where Eqn. **(2)** or Eqn. **(3)** was used for the fit, τ_e is often ill-defined due to the relatively small contributions made by the second terms of Eqn. **(2)** and Eqn. **(3)**. Thus, in many instances, it was only possible to establish an upper limit on τ_e. Also, for residues with R_{2ex} included in the fit, derived R_{2ex} values that are ≤ 1.0 s^{-1} must be regarded as insignificant, since in these cases the errors do not preclude R_{2ex} = 0.0 s^{-1}.

Most of the characterized HN sites in human profilin yield evidence of highly ordered conformations on both the ps–ns and μs–ms timescales. The average S^2 is 0.90 ± 0.09, and 81 residues do not display any significant (> 1.0 s^{-1}) exchange contributions to R_2. The S^2 values, which are related to the angular restrictions of ps–ns timescales motions, are shown mapped on to a ribbon diagram of the human profilin solution structure [10] in Fig. 2a. Regions showing uniformly high S^2 values include the N-terminal α-helix through β-strand A (residues 4–22); most residues within the second α-helix (residues 44–51) and the surrounding irregular loops (residues 36–43, 52–57); β-strand C through β-strand E (residues 63–90); β-strand F through β-strand G (residues 99–118); and most of the C-terminal α-helix (residues 123–137). Residues showing significantly reduced S^2 values ($S^2 \leq \langle S^2 \rangle - 0.09$) include Asp^{26} (S^2 = 0.65), Ser^{27} (S^2 = 0.49) and Ser^{29} (S^2 = 0.81), which are within an irregular loop connecting β-strands A and B. Also displaying reduced S^2 values are Val^{60} (S^2 = 0.81) and Asn^{61} (S^2 = 0.80) of a loop preceeding β-strand C; Thr^{92} (S^2 = 0.43), Gly^{93} (S^2 = 0.73), Gly^{94} (S^2 = 0.71) and Ala^{95} (S^2 = 0.77) of a loop between β-strands E and F; and Leu^{122} (S^2 = 0.74) at the beginning of the C-terminal α-helix. All of the residues displaying enhanced mobilities on the ps–ns timescale are in relatively exposed regions of the structure (Fig. 2A).

Fig. 2B shows the measured R_{2ex} values mapped on to profilin's backbone fold. Significant R_{2ex} values (> 1.0 s^{-1}), which are indicative of μs–ms timescale transitions among ^{15}N nuclear environments that produce different ^{15}N chemical shifts, have been obtained for 30 residues. Included among the residues displaying significant R_{2ex} values are Ala^{32} (R_{2ex} = 4.0 s^{-1}) of β-strand B; Asp^{75} (R_{2ex} = 2.5 s^{-1}), Leu^{77} (R_{2ex} = 2.9 s^{-1}), Asp^{80} (R_{2ex} > 9.0 s^{-1}) and Gly^{81} (R_{2ex} > 9.0 s^{-1}) of a loop between β-strands D and E; and Ser^{84} (R_{2ex} = 9.1 s^{-1}) and Met^{85} (R_{2ex} = 4.8 s^{-1}) of β-strand E. Large exchange contributions (R_{2ex} > 6.0 s^{-1}) are also observed for Gly^{121} of a loop proceeding the C-terminal helix, and Gln^{138} near the C-terminus. As with the faster motions, residues showing enhanced mobilities on the μs–ms

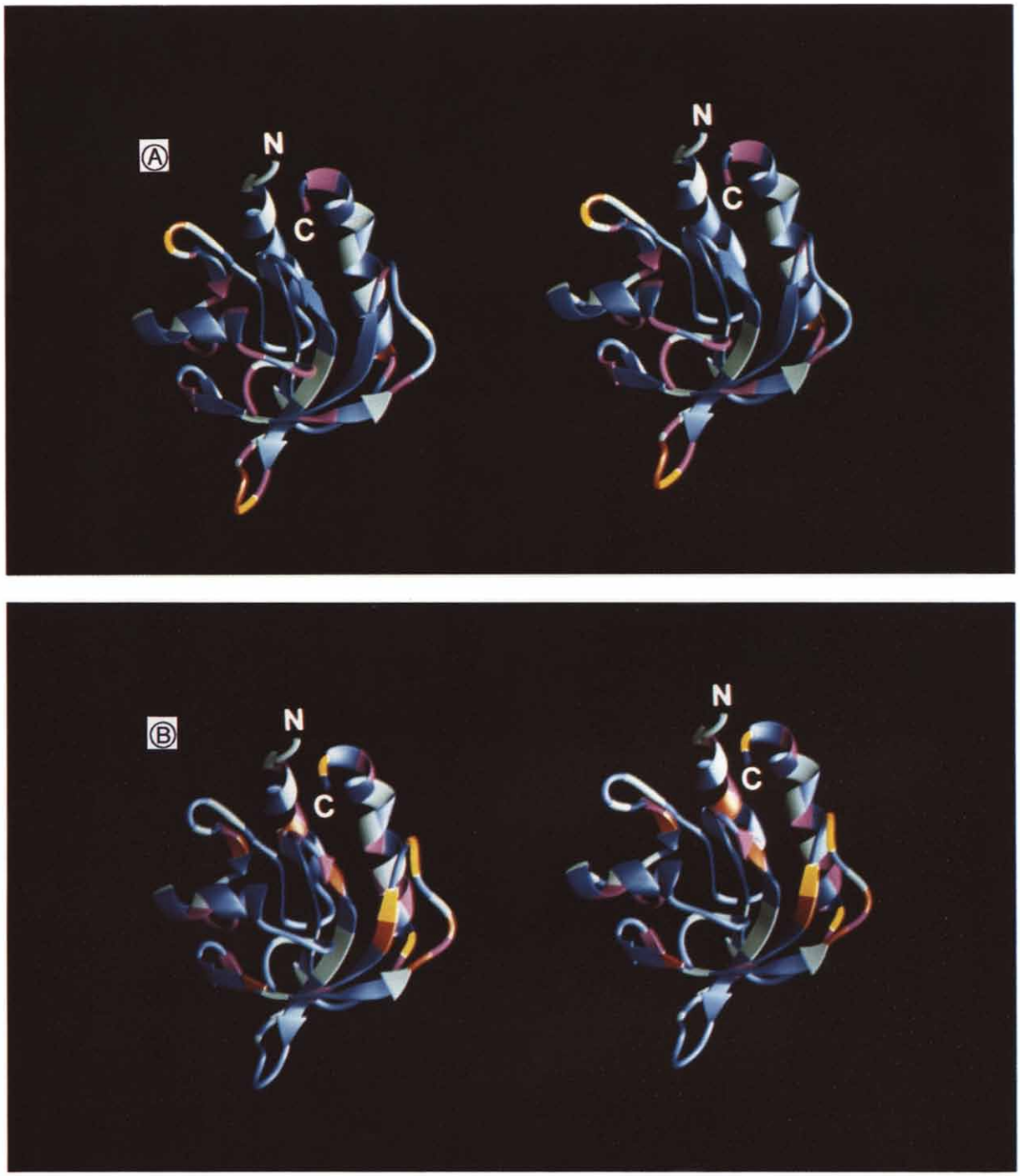

Fig. 2. Stereoviews of the human profilin backbone fold [10] – mapping of relaxation parameters. Panel A: total generalized order parameter S^2. Residue with $S^2 \geq 0.90$ are shown in blue, those with $0.90 > S^2 \geq 0.80$ are shown in maroon, those with $0.80 > S^2 \geq 0.60$ are shown in orange, and those with $S^2 < 0.60$ are shown in yellow. Panel B: exchange contributions to transverse relaxation rates. Residues with $R_{2ex} \leq 1.0\ s^{-1}$ are shown in blue, those with $1.0\ s^{-1} < R_{2ex} \leq 2.0\ s^{-1}$ are shown in maroon, those with $2.0\ s^{-1} < R_{2ex} \leq 6.0\ s^{-1}$ are shown in orange, and those with $R_{2ex} > 6.0\ s^{-1}$ are shown in yellow. For both panels, uncharacterized residues are shown in grey, and the N- and C-terminal are labeled.

timescale generally correspond to the more exposed regions of the structure (Fig. 2B).

It is informative to compare the result of this study to reported chemical shift changes induced by PLP binding [9]. Among the regions sensitive to PLP binding is the irregular loop between β-strands A and B which, as noted above, is highly dynamic on the ns timescale. Ala^{32}, Gln^{138} and the irregular loop between β-strands D and E, which display evidence of significant μs–ms timescale motions, are also perturbed by PLP binding. The high mobilities observed for some of the residues involved in PLP binding [9] indicate that induced or

selected fit of the backbone conformation may play a role in PLP/profilin interactions.

Residues within the stretch Ile^{123}–Ser^{137} (profilin's C-terminal helix) have been implicated in actin binding [26,27]. The evidence supporting this contention includes the results of chemical cross-linking studies [26], studies of peptides binding to actin [27], and the X-ray structure of gelsolin complexed with actin [28]. The involvement of profilin's C-terminal helix in actin-binding has recently been confirmed by the X-ray crystal structure of the bovine profilin/actin complex [13]. We find that this region is relatively rigid on the examined timescales, with all residues displaying S^2 values ≥ 0.85 and no residues displaying R_{2ex} values $> 1.7\ s^{-1}$. These results suggest that significant changes in the backbone conformation of profilin's C-terminal helix upon actin binding may be unlikely. The X-ray analysis of the bovine profilin/actin complex [13] revealed additional residues within the loop preceeding the C-terminal helix that also interact with actin; these include the conserved, R_2 exchange-active residue Gly^{121}. The flexibility observed in this latter region may play a role in actin-binding.

In conclusion, by allowing distinctions to be made between relatively ordered and relatively disordered regions, the characterization of profilin's backbone dynamics is expected to assist efforts aimed at obtaining a high resolution solution structure of uncomplexed human profilin. In addition, these data will serve as a reference for elucidating dynamical changes induced by interactions, such as the binding of PLP and PIP_2.

REFERENCES

[1] Haarar, B.K. and Brown, S.S. (1990) Cell Motil. Cytoskeleton 17, 71–74.

[2] Goldschmidt-Clermont, P.J. and Janmey, P.A. (1991) Cell 66, 419–421.

[3] Mockrin, S.C. and Korn, E.D. (1980) Biochemistry 31, 5117–5127.

[4] Goldschmidt-Clermont, P.J., Machesky, L.M., Doberstein, S.K. and Pollard, T.D. (1991) J. Cell Biol. 113, 1081–1089.

[5] Lassing, I. and Lindberg, U. (1985) Nature 314, 472–474.

[6] Goldschmidt-Clermont, P.J., Machesky, L.M., Baldassare, J.J. and Pollard, T.D. (1990) Science 247, 1575–1578.

[7] Tanaka, M. and Shibata, H. (1985) Eur. J. Biochem. 151, 291–297.

[8] Kaiser, D.A., Goldschmidt-Clermont, P., Levine, B.A. and Pollard, T.D. (1989) Cell Motil. Cytoskeleton 14, 251–262.

[9] Metzler, W.J., Bell, A.J., Ernst, E., Lavoie, T. and Mueller, L. (1993) J. Biol. Chem., in press.

[10] Metzler, W.J., Constantine, K.L., Friedrichs, M.S., Bell, A.J., Ernst, E.G., Lavoie, T.B. and Mueller, L. (1993) Biochemistry, in press.

[11] Magnus, K.A., Latman, E.E., Kaiser, D.A. and Pollard, T.D. (1988) Biophys. J. 53, 28a.

[12] Schutt, C.E., Lindberg, U., Myslik, J. and Strauss, N. (1989) J. Mol. Biol. 209, 735–746.

[13] Schutt, C.E., Myslik, J.C., Rozyckl, M.D., Goonesekere, N.C.W. and Lindberg, U. (1993) Nature 365, 810–816.

[14] Archer, S.J., Vinson, V.K., Pollard, T.D. and Torchia, D.A. (1993) Biochemistry 32, 6680–6687.

[15] Vinson, V.K., Archer, S.J., Lattman, E.E., Pollard, T.D. and Torchia, D.A. (1993) J. Cell Biol. 122, 1277–1283.

[16] Bjorkegren, C., Rozyckl, M.D., Schutt, C.E., Lindberg, U. and Karlsson, R. (1993) FEBS Lett. 333, 123–126.

[17] Nirmala, N.R. and Wagner, G. (1988) J. Am. Chem. Soc. 110, 7557–7558.

[18] Kay, L.E., Torchia, D.A. and Bax, A. (1989) Biochemistry 28, 8972–8979.

[19] Kay, L.E., Nicholson, L.K., Delaglio, F., Bax, A. and Torchia, D.A. (1992) J. Magn. Reson. 97, 359–375.

[20] Lipari, G. and Szabo, A. (1982) J. Am. Chem. Soc. 104, 4546–4559, 4559–4570.

[21] Clore, G.M., Szabo, A., Bax, A., Kay, L.E., Driscoll, P.C., Gronenborn, A.M. (1990) J. Am. Chem. Soc. 112, 4989–4991.

[22] Clore, G.M., Driscoll, P.C., Wingfield, P.T. and Gronenborn, A.M. (1990) Biochemistry 29, 7387–7401.

[23] Constantine, K.L., Friedrichs, M.S., Goldfarb, V., Jeffrey, P.D., Sheriff, S. and Mueller, L. (1993) Proteins Struct. Funct. Genet. 15, 290–311.

[24] Abragam, A. (1961) The Principles of Nuclear Magnetism, Clarendon Press, Oxford, UK.

[25] Press, W.H., Flannery, B.P., Teukolsky, S.A. and Veterling, W.T. (1989) Numerical Recipies: The Art of Scientific Computing, Cambridge University Press, Cambridge, UK.

[26] Vandekerckhove, J.S., Kaiser, D.A. and Pollard, T.D. (1989) J. Cell Biol. 109, 619–626.

[27] den Hartigh, J.C., van Bergen en Henegouwen, P.M.P., Verkleij, A.J. and Boonstra, J. (1992) J. Cell Biol. 119, 349–355.

[28] McLaughlin, P.J., Gooch, J.T., Mannherz, H.G. and Weeds, A.G. (1993) Nature 364, 685–692.